Supporting Information

Wang et al. 10.1073/pnas.1311543110

SI Text

Synthesis of Metallic Nanorods. The procedure for growing bimetallic nanorods (nanomotors) was adopted and modified from earlier reports (1). Anodic alumina membranes (AAO, purchased from Whatman Inc., 200 nm pore size) were used as the template for the electrodeposition of metals. We evaporated 5 nm of Cr and 350 nm of Ag by using a Kurt Lesker Lab-18 electron beam evaporator on the back side (branched pore side) of the AAO membrane to serve as the working electrode. A two-electrode system was generally used, with a Pt coil serving as both the pseudoreference electrode and the counterelectrode. When the cell was used in this configuration, electrodeposition was done at constant current. The metal plating solutions were purchased from Technic Inc. and were used as received. Metals of interest were sequentially electrodeposited into the AAO membrane, and the length of the metal segments was controlled by monitoring the charge passed. After the electrodeposition step, the membrane was thoroughly rinsed with deionized (DI) water and dried, and was soaked sequentially in 1:1 vol/vol HNO_3 and 0.5 M NaOH to dissolve the silver backing and the alumina membrane, respectively. After that the wires were sonicated and washed in DI water several times until the pH was neutral.

Gold microparticles (AuMP, 0.8–1.5 µm, 99.96%+) were purchased from Alfa Aesar. We purchased 1.7 µm polystyrene spheres from Bangs Laboratories, Inc. (PS 04N), we purchased 1.5 µm amine functionalized polystyrene spheres from Invitrogen (SKU A37324).

Finite Element Simulations. The finite element simulation model was based on two previous reports by Posner and coworkers (2, 3), and the details of the model can be found in our recently published paper (1). In this model, protons are generated and consumed at the Pt and Au ends of the nanorod (3 µm long and 300 nm in diameter), respectively, at a constant flux (7×10^{-6} mol/m^2·s). As a result of the distribution of the positively charged protons, an electric field is generated that points from the Pt end to the Au end. Because the nanorod carries a negative surface potential (–50 mV), the electric field leads to a surface electroosmotic flow along the long axis of the nanorod from Pt to Au. The distribution of ions and electrical charges as well as the fluid flow were simulated simultaneously by COMSOL, and in the end the fluid flow profile around the nanorod was generated by the simulation. Then the method developed by Solomentsev and Anderson was used to obtain the motor speed based on the fluid velocity around the nanorod (4).

1. Wang W, Chiang T-Y, Velegol D, Mallouk TE (2013) Understanding the efficiency of autonomous nano- and microscale motors. *J Am Chem Soc* 135(28): 10557–10565.
2. Moran JL, Posner JD (2011) Electrokinetic locomotion due to reaction-induced charge auto-electrophoresis. *J Fluid Mech* 680:31–66.
3. Moran JL, Wheat PM, Posner JD (2010) Locomotion of electrocatalytic nanomotors due to reaction induced charge autoelectrophoresis. *Phys Rev E Stat Nonlin Soft Matter Phys* 81(6 Pt 2):065302.
4. Solomentsev Y, Anderson JL (1994) Electrophoresis of slender particles. *J Fluid Mech* 279:197–215.

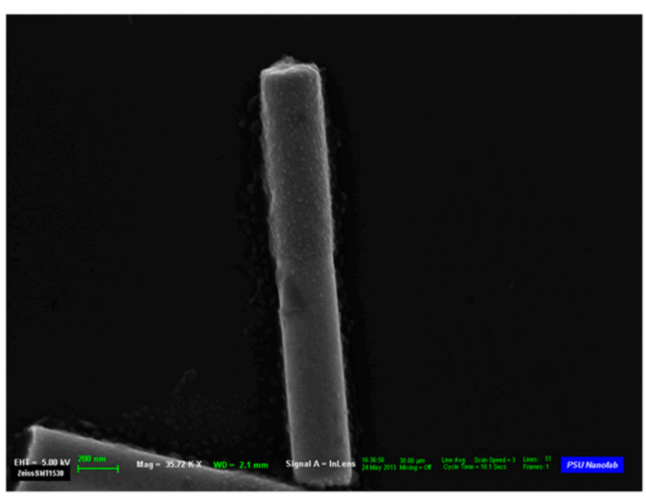

Fig. S1. Field emission SEM image of a typical Au–Pt nanorod fabricated by electrodeposition in an AAO membrane (top, Au; bottom, Pt).

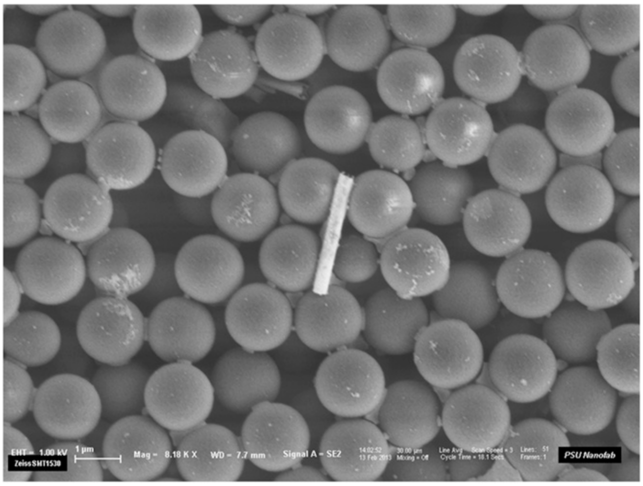

Fig. S2. Field emission SEM image (in secondary electron mode) of an Au–Pt nanorod amid an aggregate of 1.7 µm polystyrene spheres. Note that the nanorod and PS spheres are not necessarily attached together by interactions in the liquid suspension; the evaporation of the solvent exerts strong capillary forces that are likely to disrupt such interactions.

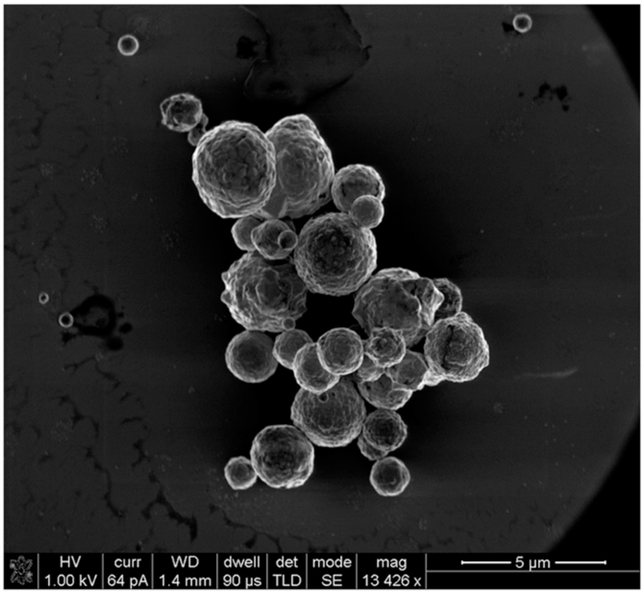

Fig. S3. Field emission SEM image of gold microspheres purchased from Alfa Aesar.

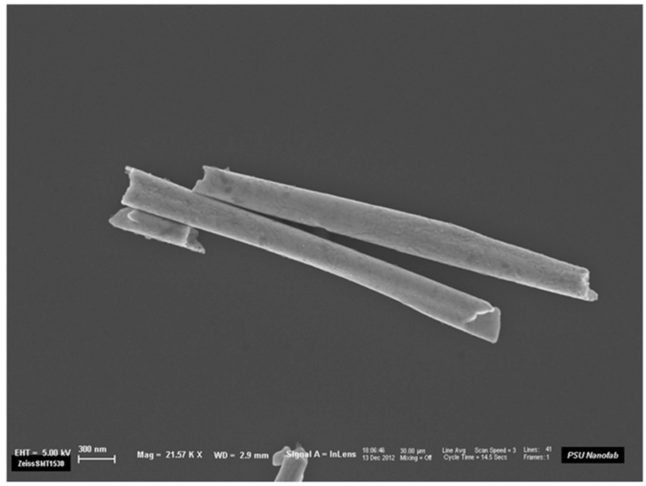

Fig. S4. Field emission SEM of a typical Au nanorod fabricated by electrodeposition in an AAO membrane.

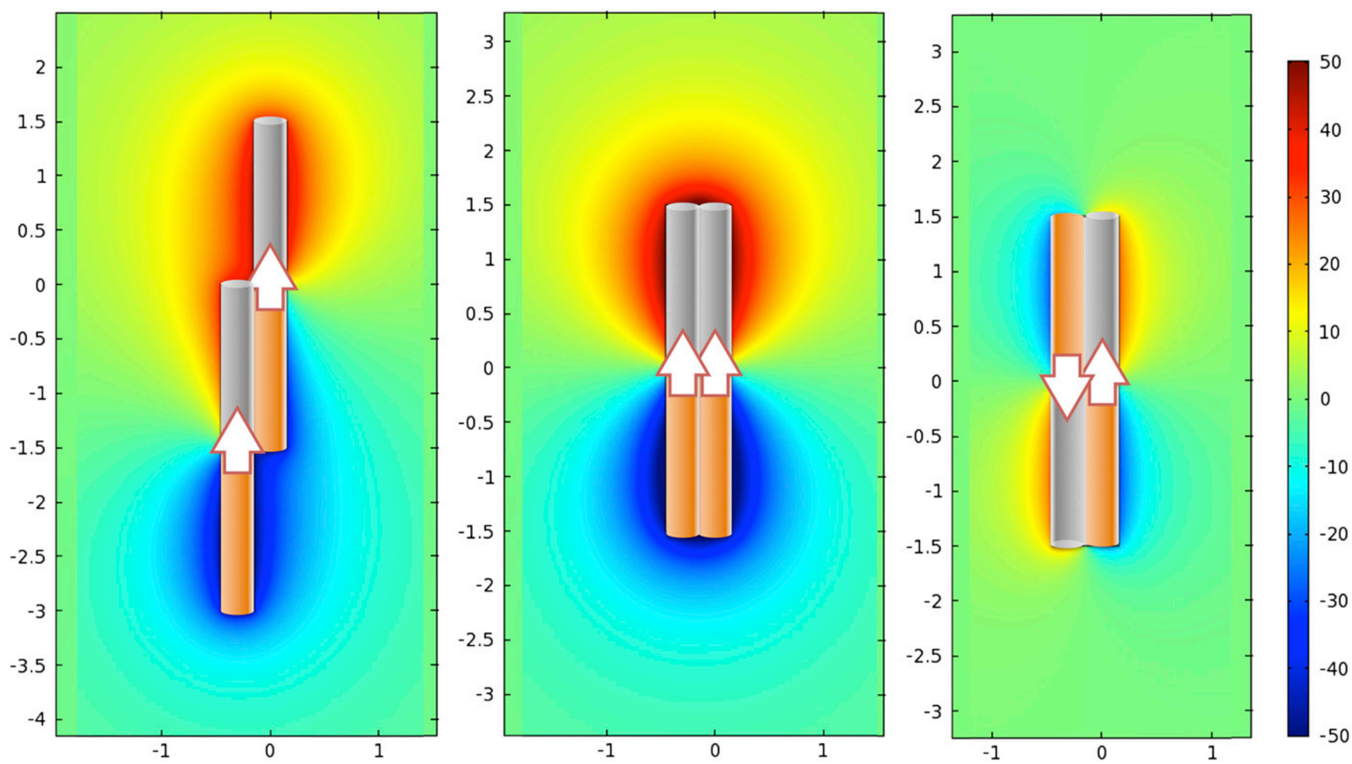

Fig. S5. Numerical simulation of the electrostatic interactions between pairs of contacting nanomotors. Distances on both *x* and *y* axes in the images are shown in μm. These images are slices of the *xz* planes of 3D simulation results. Colors in the images represent the space charge density (C/m^3), with red being positive and blue negative. (*Left*) Staggered doublet of rods moving in the same direction. (*Center*) Aligned rods moving in the same direction. (*Right*) Rods moving in opposite directions.

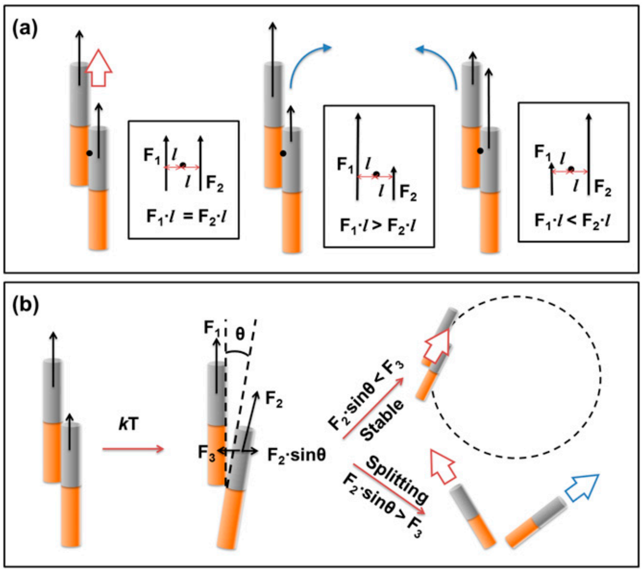

Fig. S6. Likely trajectories for a doublet composed of two Au–Pt nanomotors. (*A*) The doublet can have a linear or circular trajectory depending on the relative speed (and therefore the propulsion force, F) of the two component nanorods. Black arrows indicate the force vectors. F_1 and F_2 represent the axial propulsion force. The black dots indicate the center of drag, and *l* is the distance between it and the rod axes. (*B*) The effect of Brownian motion and propulsion force on the doublet. F_3 is the combined attractive forces that pull nanorods together (electrical and van der Waals forces). *k*T represents the thermal energy that is responsible for Brownian motion, and θ is the angle between the two nanorods. Depending on the relative magnitude of the attractive force and the random Brownian force, the doublet can maintain a stable circular path or disintegrate.

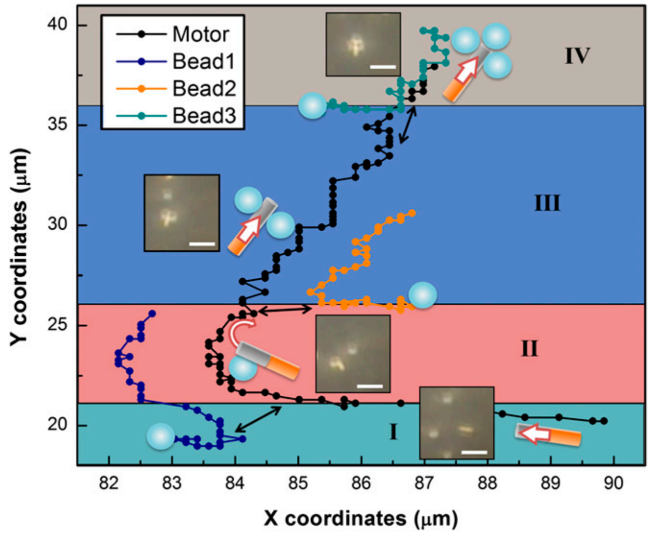

Fig. S7. Tracking results for the assembly of three polystyrene microspheres on an Au–Pt nanomotor from Movie S4. The black arrows indicate the points at which the spheres first attach to the nanomotor surface. The gaps between the trajectories of bead-1,2 and the motor represent the displacement of the centers of the particles being tracked. I, free motor; II, motor + bead-1; III, motor + bead-2; IV, motor + bead-3. The time interval between two consecutive data points is 0.033 s. (*Insets*) Optical microscopic snapshots of the assembly process. (Scale bar, 5 μm.)

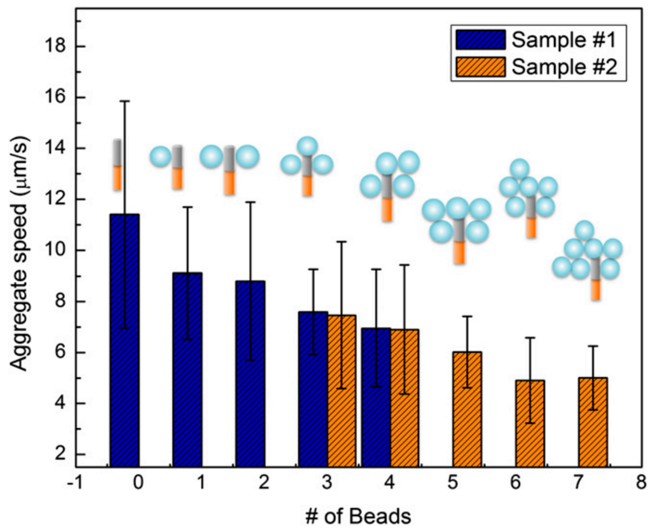

Fig. S8. The speed of nanomotor–PS aggregates with different numbers of microspheres attached to the motor surface. Two samples were analyzed. Error bars reflect one SD of the aggregate speed.

Movie S1. Illustrations of Au–Pt motor–motor interactions and the formation of rotating doublets as well as a triplet. This movie plays at 20% of the original speed, and comments are added to highlight the interaction events. This movie was taken at an overall magnification of 500×.

Movie S1

Movie S2. Interactions between active Au–Pt nanomotors and passive Au nanorods. Au–Pt nanomotors move with Pt end (silvery color) forward at ~20 μm/s, whereas Au nanorods move only slightly due to Brownian motion. This movie was taken at an overall magnification of 500×.

Movie S2

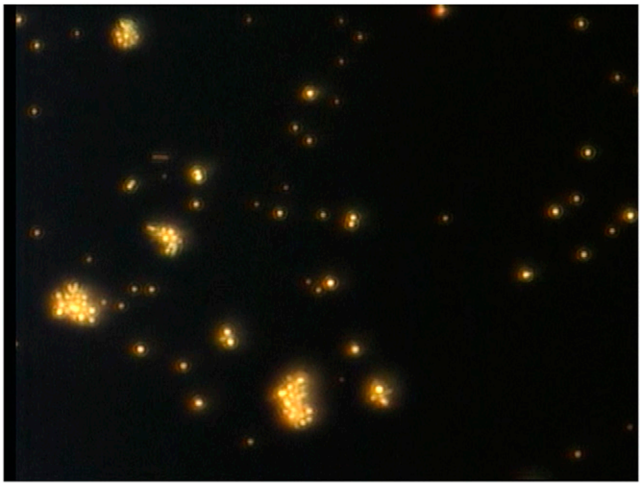

Movie S3. Interactions between active Au–Pt nanomotors and passive Au microspheres. Au–Pt nanomotors move with Pt end forward at ~20 μm/s, whereas microspheres move only slightly due to Brownian motion. Some aggregates of Au spheres and Au–Pt motors have already formed, as this movie was taken a short time after the samples were mixed. This movie was taken at an overall magnification of 500×.

Movie S3

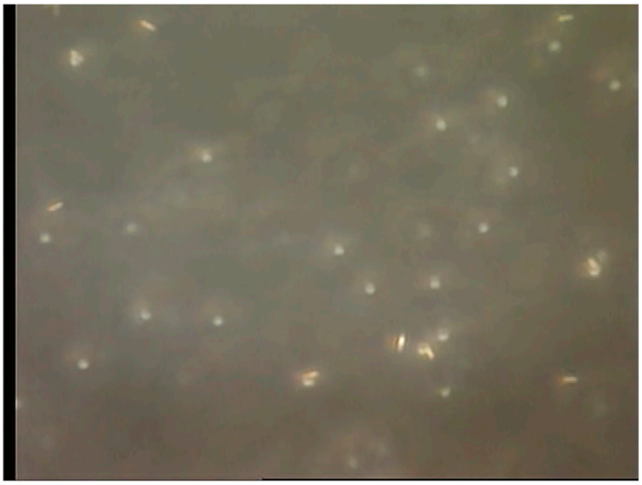

Movie S4. Interactions between one active Au–Pt nanomotor and four polystyrene spheres. The last PS sphere is picked up by the nanomotor at ~8s. This movie was taken at an overall magnification of 500×.

Movie S4

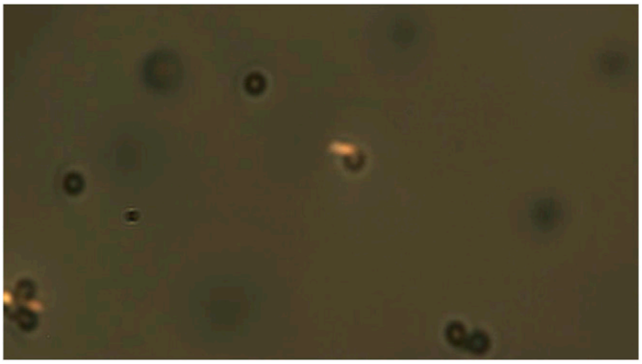

Movie S5. Rotation of an Au–Pt nanomotor with an amidine-functionalized PS sphere attached on the Au (golden color) segment. This movie was taken at an overall magnification of 1,000×.

Movie S5

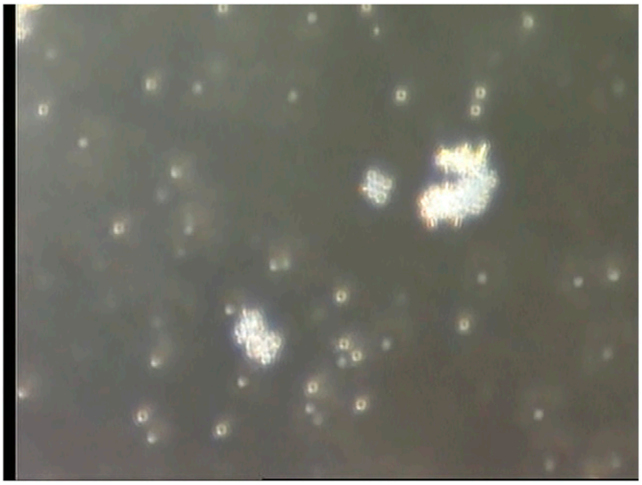

Movie S6. Example of an Au–Pt nanomotor pushing a large aggregate consisting of both Au–Pt nanorods and polystyrene spheres. This movie was taken at an overall magnification of 500×.

Movie S6